DOI: 10.30511/pcdp.2026.2073824.1050 - ISSN: 3060-8376 - Vol 3(2), 2026

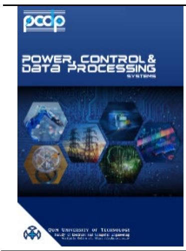

POWER, CONTROL AND DATA PROCESSING SYSTEMS

Available Online at: https://pcdp.qut.ac.ir/

A Compact Quad-Band Monopole Antenna for 5G and Wi-Fi Applications

ARTICLE INFO

Article Type
Original Research

Authors
Amir amini[1]
Mousa Abdollahvand [1,*]
Mahdi Nooshyar[1]
Sima Sobhi-Givi[1]

[1] Department of Electrical and Computer Engineering, university of Mohaghegh Ardabili (UMA), Ardabil, IRAN.

**** Correspondence***
Department of Electrical and Computer Engineering, university of Mohaghegh Ardabili (UMA), Ardabil, IRAN
(m.abdollahvand@uma.ac.ir)

Article History
Received: October 12, 2025
Accepted: February 12, 2026
ePublished: June 01, 2026

ABSTRACT

This research paper details the design and simulation of a miniaturized patch antenna with compact dimensions of 12 × 16 millimeters and a minimal profile of 1 millimeter. The developed antenna is engineered to operate effectively across multiple distinct frequency bands: 2.5 GHz, 3.8 GHz, 5.4 GHz, and 6.9 GHz. Its innovative and optimized structural configuration allows it to support a wide range of multi-band telecommunication applications, including Wi-Fi networks, 5G connectivity, and various other modern wireless technologies. A comprehensive performance evaluation was conducted using advanced electromagnetic simulation tools to analyze critical antenna parameters. The results thoroughly investigated characteristics such as gain, operational bandwidth, and impedance matching, consistently demonstrating robust and desirable performance metrics at all the specified target frequencies. Consequently, due to its highly compact form factor and proven multi-band operational capability, this antenna presents a highly suitable and efficient solution for integration into space-constrained portable devices and the next generation of modern communication systems, addressing the growing demand for versatile and miniaturized RF components.

Keywords: antenna; multi-band; frequency; MIMO.

1 Introduction

With the ever-increasing demand for wireless services and the emergence of 5G technology alongside the Internet of Things (IoT), it is anticipated that data exchange among users of these systems will significantly increase [1]. Among the key components in communication systems capable of meeting the demands of 5G technology is the antenna. Antennas are designed in two configurations: single-element and multi-element. Most antenna designs presented in the research literature are based on a single-element structure. However, single-element antennas have performance limitations in terms of parameters such as gain and bandwidth. MIMO (Multiple-Input Multiple-Output) antenna systems have emerged as an efficient solution for meeting the high-speed requirements of modern communication networks. In this configuration, multiple antenna elements are arranged on a single substrate, with each element fed by its dedicated port. All ports can operate simultaneously on the same carrier frequency, with each port responsible for transmitting a portion of the system's data [2, 3]. Various designs of MIMO antennas with diverse features have been presented in research articles and sources [4-6]. Two-element [7, 8], four-element [4, 9-10], six-element [11], and other configurations can be used in MIMO antenna design. One of the most widely used MIMO designs is the four-element system. A four-element MIMO antenna can be organized in a linear or rectangular configuration. In one notable MIMO design, researchers in reference [9] proposed a single annular ring patch that can act as a single radiator for four ports; in other words, a four-element MIMO antenna was designed using a single radiator. Generally, a MIMO antenna system is built so that each port can be a single-element antenna or an array of antennas. In reference [12], a two-port MIMO system is presented where each port includes a four-antenna array with a corporate feed network. Recently, the concept of Massive MIMO systems has been employed for MIMO antennas with a very large number of elements, representing an important component of future wireless technology [13, 14]. Regarding the operational frequency band, some MIMO designs have considered lower frequency bands, i.e., below 1 GHz [15, 16]; however, certain frequency bands have attracted more attention from researchers due to their importance, including sub-6 GHz bands [12, 17, 18]. For example, in reference [18], a four-port antenna is proposed where the four ports are located at the four corners of a flexible substrate with a shared ground plane in the center between them. Each antenna port was designed as four octagonal loops between two conductive layers with a T-shape. The antenna structure was equipped with L-shaped and E-shaped conductive elements optimized for the antenna's operation in a wide frequency band (2.37 to 5.85 GHz). In addition to single-band MIMO antennas, multi-band MIMO antennas can also be designed [19, 20]. In reference [21], a reconfigurable dual-band antenna operating in the ranges of 1.3 to 1.8 GHz and 1.8 to 2.6 GHz is investigated. Tri-band MIMO systems can be found in references [22, 23]. Furthermore, Ultra-Wideband (UWB) MIMO antennas have been introduced in references [24, 25]. In this design, we also utilized 4 modified U-shaped elements on the front of the antenna and an integrated claw-shaped parasitic element on the back of the antenna to achieve our goals. The antenna size is 16mm×12mm×1mm; its small size is very notable and, as a multi-band antenna, it can have various applications.

2 Initial Patch Dimension (Width & Length):

The starting point for a rectangular patch antenna operating at the fundamental TM_{10} mode is calculating its width (W) and length (L). The width primarily affects the input impedance and radiation efficiency, while the length is directly tied to the resonant frequency.

1. Patch Width (W):

$$W = \frac{c}{2\,F_r\,\sqrt{\epsilon_r}}\sqrt{\frac{2}{\epsilon_r+1}} \qquad \text{Eq 1}$$

where `c` is the speed of light, `$f_r$` is the target resonant frequency, and `$\epsilon_r$` is the dielectric constant of the substrate.

2. Effective Dielectric Constant (ϵ_eff): Due to fringing fields, the patch appears to be on a substrate with an effective dielectric constant.

$$\epsilon_{eff} = \frac{\epsilon_r+1}{2} + \frac{\epsilon_r-1}{2}\left(1+12\frac{h}{w}\right)^{-1/2} \qquad \text{Eq2}$$

where `h` is the substrate thickness.

3. Length Extension (ΔL): Fringing fields make the electrical length of the patch slightly longer than its physical length.

$$\Delta L = 0.412h\frac{(\epsilon_{eff}+0.3)\left(\frac{w}{h}+0.264\right)}{(\epsilon_{eff}+0.258)\left(\frac{w}{h}+0.8\right)} \qquad \text{Eq3}$$

4. Patch Length (L):

$$L = \frac{c}{2f_r\sqrt{\epsilon_{eff}}} - 2\Delta L \qquad \text{Eq4}$$

2.1 Design and shape

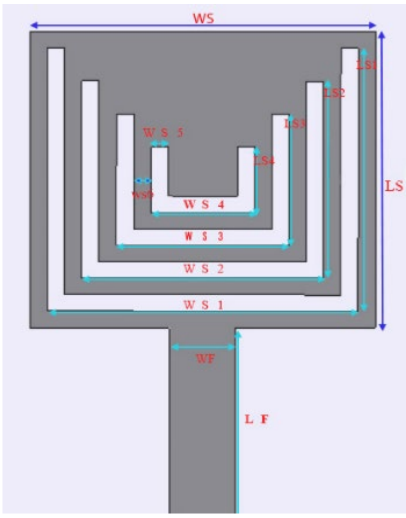

Figure 1: Front layout of the antenna indicating the design parameters.

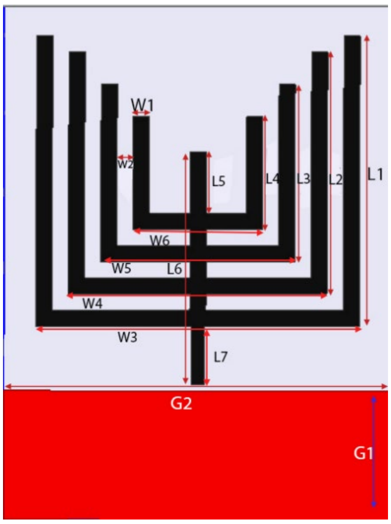

Figure 2: back layout of the antenna indicating the design parameters.

The dimensions specified in the figure are as follows:
Ws =10mm , Ls =9mm , wf=1.91mm ,Lf=6mm,
Ws1=9mm, ws2=7mm ,ws3=5mm ws4=3mm
Ws5=0.5mm ,ws6=0.5mm ,LS1=8mm
LS2=6mm ,LS3=4mm,LS4=2mm,L4=3.5mm
G1=4mm ,G2=12mm , L1=9 mm,
L2=7.5mm,L3=5.5mm,L5=1.9mm
L6=7.2mm,w1=0.5mm w2=0.5mm
W3=10mm, w4=8mm,w5=6mm,w6=4mm
W7=0.4mm.

As you can see, in the image on the left, there is an antenna with a square design featuring modified U-shaped slots, the final dimensions of which are provided in top Additionally, behind the antenna in Figure 1, we have a partial ground plane with specific dimensions. On the back of the antenna, there is a modified fork-shaped element that is not connected to the ground plane and acts as a parasitic element to enhance the received signal strength of the antenna. All dimensions are listed in top.

3 Result

As you can see, the evolution of the antenna is presented in Figure 4. In the figure 3, the blue curve corresponds to the simple antenna structure (Antenna I), the brown curve corresponds to the second antenna structure with the two U-shaped slot design (Antenna II), and the black curve in the S11 diagram corresponds to the final structure, which exhibits multiple resonances (Final Antenna). Next, we proceed to examine the current distribution plots and the radiation pattern of the antenna at the receiving frequency.

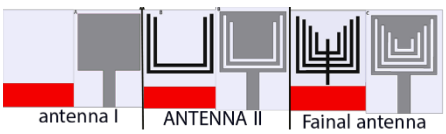

Figure3: Antenna Design Evolution: From Simple to Final Model.

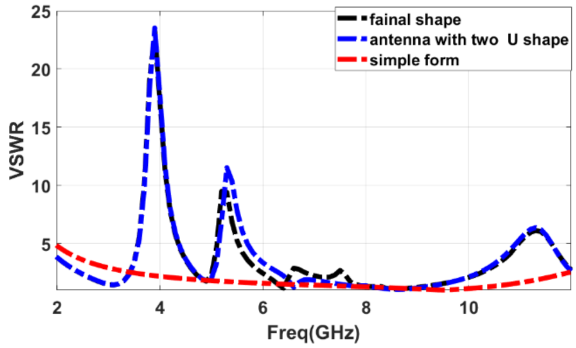

Figure4: VSWR plots showing the design evolution from the initial simple antenna to the final optimized structure

As shown in Figure 5, the progression toward multiband operation is evident in the S11 characteristics. The initial simple antenna (blue curve) exhibits single-band behavior. The incorporation of two U-shaped elements (red curve) modifies the response, while the final design (black curve) achieves multiband performance.

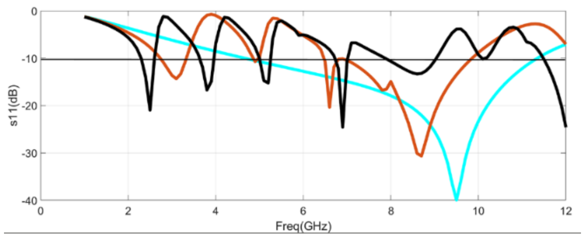

Figure 5: The S11 parameter graph illustrates the evolutionary process of multiband signal reception from the initial antenna to the final design

The surface current distribution in Figure 6 reveals that the elements with the highest current density (shown in red) are the primary drivers of the antenna's performance at the target frequencies. A key example is visible in Figure 6, where the strong current concentration on the partial ground plane and the fork-shaped slot directly facilitates resonance at 6.9 GHz.

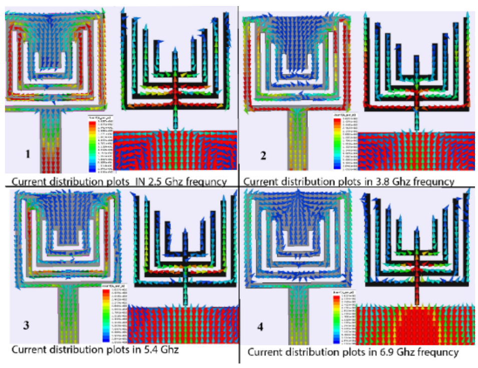

Figure 6: The behavior of the antenna in the current distribution plot at different frequencies.

The radiation pattern of a microstrip antenna serves as a fundamental indicator for evaluating the performance of these antennas for modern communication systems. At the specified frequency bands of 2.5, 3.8, 5.4, and 6.9 GHz, the radiation characteristics are influenced by three key factors: waveguide effects due to the antenna's structure, dielectric losses in the substrate, and the complex coupling behavior between radiating elements. These characteristics make far-field radiation pattern analysis critical for optimizing communication links.

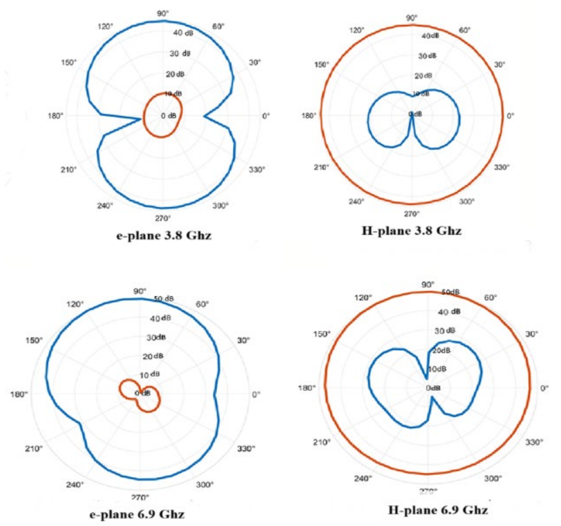

Figure 7 : Radiation pattern (E-plane and H-plane) of the antenna in question at 3.8Ghz and 6.9Ghz operating frequencies.

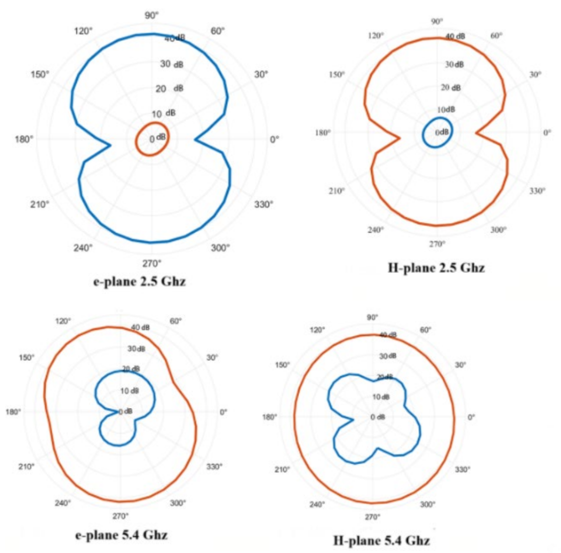

Figure 8 : Radiation pattern (E-plane and H-plane) of the antenna in question at 2.5Ghz and 5.4 Ghz operating frequencies.

The most significant features of the radiation pattern for communication applications include a configurable beamwidth, which enables a strategic balance between wide-area coverage and high-directivity links across the different bands. For instance, a wider beam at 2.5 GHz is suitable for broader coverage, while a narrower beam at 5.4 and 6.9 GHz is ideal for high-capacity point-to-point connections. Low side lobe levels in these antennas are essential for reducing interference in dense communication environments and can be achieved through the optimization of the patch geometry and array configuration. Precise control of polarization (linear/circular) provides the necessary flexibility to adapt to different communication protocols and mitigate polarization mismatch in urban and indoor environments. Gain is a central characteristic of these antennas, directly influenced by the optimized design of the patch structure and ground plane, which is critical for ensuring strong signal strength and link reliability across the target frequencies. In this research, the impact of structural parameters, including substrate material and thickness, patch geometry, and array configuration on the radiation pattern characteristics at 2.5, 3.8, 5.4, and 6.9 GHz is thoroughly investigated. Furthermore, considering practical applications, the stability of the radiation pattern under varying environmental conditions (such as changes in humidity and temperature) and its effect on signal integrity and data transfer rates is a key focus of the analysis. The proposed antenna design demonstrates a robust and versatile radiation pattern across the operational bands. It achieves a highly focused main lobe with high gain, making it exceptionally suitable for high-throughput point-to-point communication links. Simultaneously, the design can be configured to provide a wider beamwidth for applications requiring broader sector coverage, such as in public Wi-Fi access points or cellular network base stations. This adaptability ensures reliable and efficient data transmission for a wide range of communication scenarios, from long-range backhaul links to dense urban user access.

3.1 Parametric Evaluation

Since the handle needs to be added in a parasitic form, we must find a suitable and optimal size for it. Therefore, we will conduct a parametric study of the fork handle length.

The black graph represents the final simulation results of our antenna, where we set the fork handle size at 7.2 mm. By incrementally increasing this length parameter, we compared the obtained results with the original antenna, but the initial outcomes were unacceptable.First, we added 1 mm to the handle (represented by the +1 mm graph). We continued this process progressively until reaching 3.5 mm. To avoid cluttering the graph, only three cases are displayed. However, we can definitively state that the 7.2 mm length remains the optimal choice for all four received frequencies of the fork we added, as shown in the figure 10.

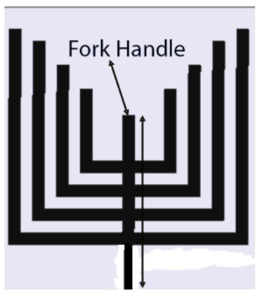

Figure 9: A view of the fork-shaped antenna parasitic element.

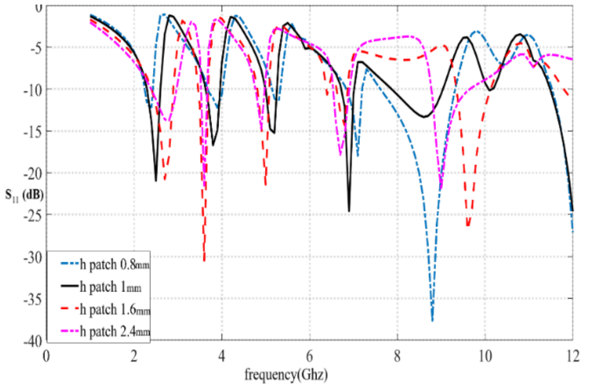

Figure 10: S11 Parameter Comparison Chart for Fork Handle Length

By comparing the patch thickness of the antenna from 0.8 mm to 2.4 mm, we observe frequency shift, gain enhancement at one or two frequencies, and attenuation at other frequencies. When comparing the proposed thickness of 1 mm with 0.8 mm, as can be seen in Figure 11, one of our nulls is enhanced while the other three are attenuated. Compared to 1.6 mm, although there is significant gain enhancement at the two middle frequencies, frequency shift is observed at the other two frequencies. In comparison with the original work using 2.4 mm thickness, only one frequency is enhanced, while the other frequencies experience attenuation along with frequency shift.

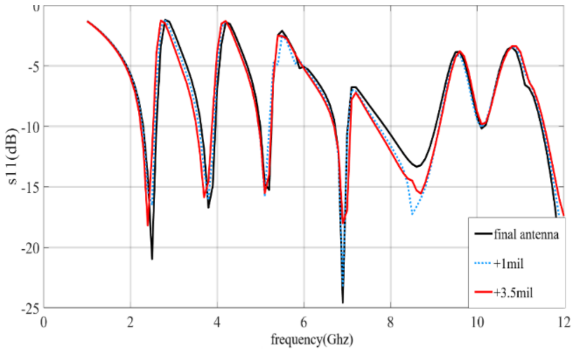

Figure 11: A table comparing S11 versus antenna thickness

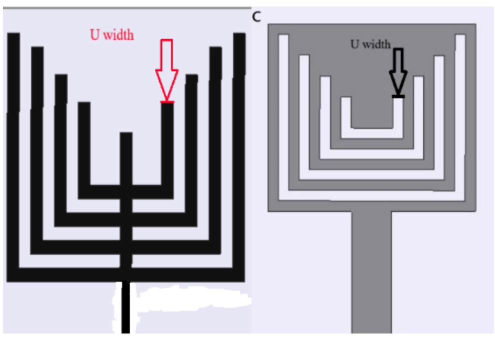

Figure 12: A View of back and top antenna and parameter we comparison.

A parametric study of the mentioned antenna element was conducted by comparing the notch width at the front and increasing the width of the claw-shaped arms at the rear. According to Figure 13 (S11 parameter), increasing the notch width and the width of the claw-shaped arms enhances the lower frequencies and attenuates the higher frequencies. Furthermore, the bandwidth in the lower frequency range increases slightly, accompanied by a minor frequency shift. In this part of the study, all parameters of the U-shaped slot were increased. The width of the claw arm was also increased. In the next part of our parametric study, we will only examine the width of the claw arm, which is shown in Figure 13.

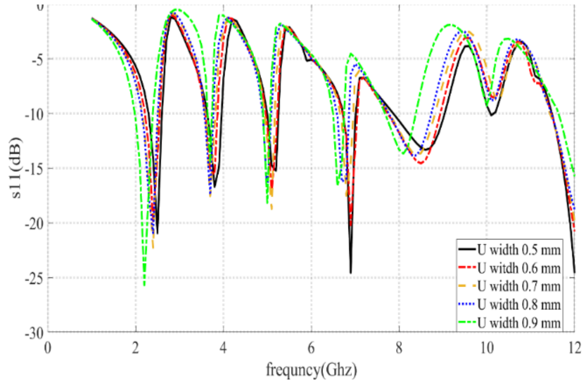

Figure13: S11 plot comparing the width of the U-shaped slots

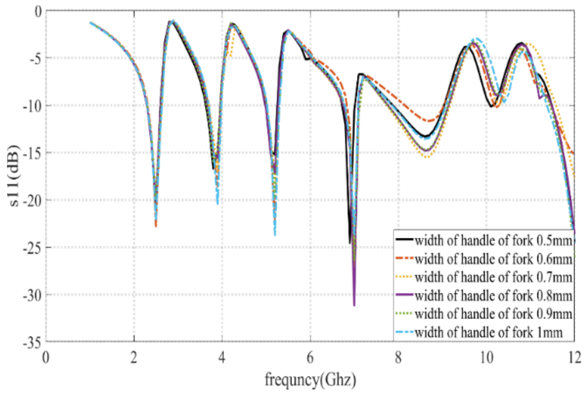

Figure13: S11 parameter plot versus the width of the U-shaped parasitic element.

A performance comparison was conducted between the primary design with a width of 0.5 mm and other widths. Compared to the 0.5 mm width, the 0.6 mm and 0.7 mm variants exhibited signal gain at the first two resonant frequencies but introduced attenuation at the two subsequent frequencies.Similarly, when benchmarked against the 0.5 mm width, the 0.8 mm and 0.9 mm configurations resulted in attenuation at both the first and third frequencies.The 1 mm width demonstrated a more pronounced gain across the first three frequencies compared to the 0.5 mm baseline. However, at the fourth frequency, its performance degraded, showing a frequency shift of 0.1 GHz accompanied by an attenuation of 2 dB.

4 Conclusion

This paper presents a compact, four-port MIMO antenna designed for multi-band operation in modern wireless systems.

The final design, featuring four modified U-shaped radiators and an optimized claw-shaped parasitic element, successfully achieves resonant frequencies at 2.5, 3.8, 5.4, and 6.9 GHz. A parametric study confirmed the optimal dimensions for robust performance. The antenna exhibits favorable radiation patterns with stable gain and directivity across all bands, making it a suitable and efficient candidate for 5G and IoT applications where small size and multi-band functionality are critical.

Disclosure of Potential Conflicts of Interest

The Authors declare that there is no conflict of interest

Reference

[1] L. Chettri and R. Bera, "A Comprehensive Survey on Internet of Things (IoT) Toward 5G Wireless Systems," *IEEE Internet Things J.*, vol. 7, no. 1, pp. 16–32, Jan. 2020, doi: 10.1109/jiot.2019.2948888.

[2] I. Khan, Q. Wu, I. Ullah, S. U. Rahman, H. Ullah, and K. Zhang, "Designed Circularly Polarized Two-Port Microstrip MIMO Antenna for WLAN Applications," *Applied Sciences*, vol. 12, no. 3, p. 1068, Jan. 2022, doi: 10.3390/app12031068.

[3] Malviya, L.; Panigrahi, R.K.; Kartikeyan, M. MIMO Antennas for Wireless Communication: Theory and Design; CRC Press: Boca Raton, FL, USA, 2020.

[4] L. Qu, H. Piao, and H. Kim, "Compact wideband MIMO mobile-antenna system design using mode-based decoupling techniques," *Int J RF Microw Comput Aided Eng*, vol. 29, no. 8, Apr. 2019, doi: 10.1002/mmce.21765.

[5] C. Deng, D. Liu, and X. Lv, "Tightly Arranged Four-Element MIMO Antennas for 5G Mobile Terminals," *IEEE Trans. Antennas Propagat.*, vol. 67, no. 10, pp. 6353–6361, Oct. 2019, doi: 10.1109/tap.2019.2922757.

[6] H. T. Chattha, "4-Port 2-Element MIMO Antenna for 5G Portable Applications," *IEEE Access*, vol. 7, pp. 96516–96520, 2019, doi: 10.1109/access.2019.2925351.

[7] Al-Fayyadh, Hussein Qasim, Abdulghafor Abdulghafar Abdulhameed, Abdulkareem Swadi Abdullah, and Haider Mohammed Alsabbagh. "Flexible (2$\times $1) MIMO antenna with electromagnetic band gap unit cell for WiMAX applications." *Turkish Journal of Electrical Engineering and Computer Sciences*, vol. 25, no. 4, 2017, 3061-3072., doi: 10.3906/elk-1603-94.

[8] A. Kumar, A. Q. Ansari, B. K. Kanaujia, J. Kishor, and S. Kumar, "An ultra-compact two-port UWB-MIMO antenna with dual band-notched characteristics," *AEU - International Journal of Electronics and Communications*, vol. 114, p. 152997, Feb. 2020, doi: 10.1016/j.aeue.2019.152997.

[9] K. R. Jha, Z. A. P. Jibran, C. Singh, and S. K. Sharma, "4-Port MIMO Antenna Using Common Radiator on a Flexible Substrate for Sub-1GHz, Sub-6GHz 5G NR, and Wi-Fi 6 Applications," *IEEE Open J. Antennas Propag.*, vol. 2, pp. 689–701, 2021, doi: 10.1109/ojap.2021.3083932.

[10] A. Biswas and V. R. Gupta, "Design and Development of Low Profile MIMO Antenna for 5G New Radio Smartphone Applications," *Wireless Pers Commun*, vol. 111, no. 3, pp. 1695–1706, Nov. 2019, doi: 10.1007/s11277-019-06949-z.

[11] D. R. Kumar and G. V. Babu, "Six-Port Quarter Wavelength Slotted MIMO Antenna for 5G Mobile Phone," *Wireless Pers Commun,* vol. 120, no. 3, pp. 2043–2059, Jul. 2021, doi: 10.1007/s11277-021-08733-4.

[12] M. A. Al-Tarifi, M. S. Sharawi, and A. Shamim, "Massive MIMO antenna system for 5G base stations with directive ports and switched beamsteering capabilities," *IET Microwaves Antenna & Prop*, vol. 12, no. 10, pp. 1709–1718, Jun. 2018, doi: 10.1049/iet-map.2018.0005.

[13] Q.-U.-A. Nadeem, A. Kammoun, M. Debbah, and M.-S. Alouini, "Design of 5G Full Dimension Massive MIMO Systems," *IEEE Trans. Commun.*, vol. 66, no. 2, pp. 726–740, Feb. 2018, doi: 10.1109/tcomm.2017.2762685.

[14] R. Hussain, S. I. Alhuwaimel, A. M. Algarni, K. Aljaloud, and N. Hussain, "A Compact Sub-GHz Wide Tunable Antenna Design for IoT Applications," *Electronics*, vol. 11, no. 7, p. 1074, Mar. 2022, doi: 10.3390/electronics11071074.

[15] Aust, Stefan, R. Venkatesha Prasad, and Ignas GMM Niemegeers. "Performance study of MIMO-OFDM platform in narrow-band sub-1 GHz wireless LANs." *In 2013 11th International Symposium and Workshops on Modeling and Optimization in Mobile, Ad Hoc and Wireless Networks (WiOpt),* pp. 89-94. IEEE, 2013.

[16] T. Alam, S. R. Thummaluru, and R. K. Chaudhary, "Integration of MIMO and Cognitive Radio for Sub-6 GHz 5G Applications," *Antennas Wirel. Propag. Lett.*, vol. 18, no. 10, pp. 2021–2025, Oct. 2019, doi: 10.1109/lawp.2019.2936312.

[17] J. Kulkarni, A. G. Alharbi, A. Desai, C.-Y.-D. Sim, and A. Poddar, "Design and Analysis of Wideband Flexible Self-Isolating MIMO Antennas for Sub-6 GHz 5G and WLAN Smartphone Terminals," *Electronics*, vol. 10, no. 23, p. 3031, Dec. 2021, doi: 10.3390/electronics10233031.

[18] M. M. Fakharian, M. Alibakhshikenari, C. H. See, and R. Abd-Alhameed, "A high gain multiband offset MIMO antenna based on a planar log-periodic array for Ku/K-band applications," *Sci Rep*, vol. 12, no. 1, Mar. 2022, doi: 10.1038/s41598-022-07866-1.

[19] T. Agrawal and S. Srivastava, "Compact MIMO Antenna for Multiband Mobile Applications," *J. Microw. Optoelectron. Electromagn. Appl.*, vol. 16, no. 2, pp. 542–552, Apr. 2017, doi: 10.1590/2179-10742017v16i2899.

[20] X. Zhao and S. Riaz, "A Dual-Band Frequency Reconfigurable MIMO Patch-Slot Antenna Based on Reconfigurable Microstrip Feedline," *IEEE Access*, vol. 6, pp. 41450–41457, 2018, doi: 10.1109/access.2018.2858442.

[21] J. Rajeshwar Goud, N. V. Koteswara Rao, and A. M. Prasad, "A NOVEL TRIPLE BAND MIMO ANTENNA ARRAY FOR SIMULTANEOUS COMMUNICATIONS," *PIER M*, vol. 102, pp. 159–169, 2021, doi: 10.2528/pierm21042205.

[22] J.-S. Sun, H.-S. Fang, P.-Y. Lin, and C.-S. Chuang, "Triple-Band MIMO Antenna for Mobile Wireless Applications," Antennas Wirel. Propag. Lett., vol. 15, pp. 500–503, 2016, doi: 10.1109/lawp.2015.2454536.

[23] W. Li, Y. Hei, P. M. Grubb, X. Shi, and R. T. Chen, "Compact Inkjet-Printed Flexible MIMO Antenna for UWB Applications," IEEE Access, vol. 6, pp. 50290–50298, 2018, doi: 10.1109/access.2018.2868707.

[24] A. S. Eltrass and N. A. Elborae, "New design of UWB-MIMO antenna with enhanced isolation and dual-band rejection for WiMAX and WLAN systems," IET Microwaves Antenna & Prop, vol. 13, no. 5, pp. 683–691, Feb. 2019, doi: 10.1049/iet-map.2018.5810.